

Near-Infrared Spectroscopy for Monitoring Starch Hydrolysis

HOEIL CHUNG* and MARK A. ARNOLD

NIR Project Team, SK Corporation, 110 Nam-Gu, Kosa-Dong, Ulsan, Korea (H.C.); and Department of Chemistry, University of Iowa, Iowa City, Iowa 52242 (M.A.A.)

Near-infrared (NIR) spectroscopy has been evaluated for monitoring the acid-catalyzed hydrolysis (thinning) of starch. In practice, the extent of starch hydrolysis is measured in fluidity units, which correspond to a physical property of the hydrolyzed starch material. NIR spectra of samples taken periodically during a series of starch-thinning reactions were used to predict fluidity. The standard error of prediction (SEP) was 1.06 mL with the use of partial least-squares (PLS) regression in conjunction with digital Fourier filtering. This SEP was significantly better than that reported before with a univariate calibration model based on the integrated area of the 4400 cm^{-1} (2272 nm) absorption band for carbohydrates. The improved SEP meets the industry demands for real-time monitoring. Although these calibration models were developed from samples prepared in the laboratory, no spectroscopic differences were apparent between spectra collected from these laboratory samples and spectra collected from samples taken directly from plant starch slurries during actual thinning reactions. This similarity in spectral features, and hence chemical matrix, supports the potential of NIR spectroscopy for *on-line* monitoring of industrial starch-thinning processes.

Index Headings: Near-infrared spectroscopy; Starch hydrolysis (thinning); Partial least-squares; Digital Fourier filter.

INTRODUCTION

Spectroscopic sensing with near-infrared (NIR) spectroscopy is rapid, nondestructive, and noncontaminating.^{1,2} These properties make NIR spectroscopy ideally suited for monitoring the acid-catalyzed hydrolysis (a process that causes thinning) of starch. Such starch-thinning reactions are used in industry to produce different types of adhesive products. The degree of starch hydrolysis is critical as it determines the physical and chemical properties of the final product. Thinning reactions are conventionally monitored by manually withdrawing samples and measuring the fluidity of the processed starch material. The *off-line* fluidity measurement is time consuming, labor intensive, and difficult to implement in an *on-line* manner.

We previously reported on the ability to following the starch hydrolysis process with NIR spectra collected from samples taken during starch hydrolysis reactions.³ A univariate calibration model was used in this earlier work to relate the integrated area under the 4400 cm^{-1} (2272 nm) carbohydrate absorption band to fluidity of the processed starch. The standard error of prediction (SEP) was 1.94 mL for the prediction of fluidity. Unfortunately, this prediction error is too high for the purposes of *on-line* process control. An SEP of 1.0 mL was required for such applications.

Carbohydrates possess three distinct absorption bands within the combination region of the NIR spectrum. These bands are centered at approximately 4700, 4400, and 4300 cm^{-1} (2128, 2272, and 2326 nm). Improvements in model prediction are expected by using a multivariate calibration method and incorporating all the carbohydrate spectral information into the model. In addition, the thinning reaction produces a mixture of complex carbohydrates, and the distribution of carbohydrates changes continuously during the hydrolysis process. This solution complexity is evident in the corresponding NIR spectra, which renders a simple univariate calibration method insufficient to resolve the subtle spectral variations observed during the thinning reaction. Again, a multivariate calibration technique^{4,5} can incorporate more of the spectral information into the model and, thus, more accurately relate spectral variations to starch fluidity.

In this paper, PLS regression was used to improve the analytical performance of NIR spectroscopy for monitoring the starch hydrolysis reaction. Our approach was motivated by the established ability of PLS to extract glucose-specific information in aqueous-based biological and clinical matrices.⁶⁻⁸ Digital Fourier filtering was used as a preprocessing step to enhance calibration performance by reducing spectral noise and baseline variations.^{6,9} With the combination of PLS with digital Fourier filtering, accurate fluidity predictions were possible with an SEP and mean percent error of 1.06 mL and 2.16%, respectively. The relationship between spectral acquisition time and prediction accuracy was evaluated. Finally, the potential of this spectroscopic technique for *on-line* process monitoring was assessed by comparing NIR spectra collected from starch slurry samples prepared in the laboratory and samples obtained during actual industrial thinning reactions.

EXPERIMENTAL

Apparatus and Chemicals. All spectra were collected with a Nicolet 740 Fourier transform infrared (FT-IR) spectrometer (Nicolet Analytical Instruments, Madison, WI). The spectrometer was designed to operate in the NIR range by using a 250 W tungsten-halogen source, CaF_2 beamsplitter, and cryogenically cooled InSb detector. To isolate the spectral range of 5000–4000 cm^{-1} (2000–2500 nm), we used a multilayer optical interference filter (Barr Assoc., Westford, MA). A 2 mm path-length rectangular cell made from Infrasil quartz (Wilma Glass Co., Buena, NJ) was used.

Sulfuric acid, sodium carbonate, and hydrochloric acid were obtained from common suppliers. Pearl starch and

Received 17 May 1999; accepted 20 September 1999.
* Author to whom correspondence should be sent.

0.375 N sodium hydroxide were supplied from A. E. Staley Mfg. Co. (Decatur, IL).

Thinning Reaction. Eleven separate thinning reactions were run in order to collect samples for analysis. For each reaction, a fresh batch of starch slurry was prepared by mixing 1.5 kg of Pearl starch in 2.0 L of water. The slurry was placed in a glass-jacketed cell and heated to between 50 and 55 °C with a VWR Model 1140 temperature bath (VWR Scientific, Chicago, IL). After the temperature stabilized, the hydrolysis reaction was initiated by slowly adding 67.2 mL of 30% sulfuric acid to the slurry over a period of one minute. For each sample, two aliquots of slurry were extracted for analysis. One aliquot (≈ 20 mL) was used for collecting the NIR spectrum and the other (≈ 150 mL) was used to determine the corresponding fluidity. Samples were collected at noted reaction times, and, in general, 10 samples were collected during each thinning reaction.

Fluidity of dried starch cakes was measured as described before.³ Briefly, the slurry sample was dried to produce a starch cake that was weighed and dissolved in concentration base. The resulting solution was placed in a closed funnel. The neck of the funnel was opened to permit the solution to flow for exactly 1 min. The volume of solution passing through the funnel during this time was measured in a graduated cylinder. The use of a graduated cylinder is standard for the industry and contributes an uncertainty of ± 0.5 mL. Smaller volumes were collected for solutions with lower fluidity and higher viscosity.

NIR Spectra. Immediately after extraction, slurry samples were immersed in an ice bath for 30 s to stop the thinning process. Cooled samples were then centrifuged at 5000 rpm for 2 min, and the resulting supernatant was filtered through a 0.45 μm polycarbonate syringe filter (Millipore, Bedford, MA). NIR spectra of the filtered supernatant were collected. Samples were placed in a water-jacketed, thermostatted cell, and the solution temperature was maintained at 20 ± 0.1 °C while spectra were collected.

All spectra were collected as 256 coadded, double-sided, 16K interferograms. This procedure resulted in spectra with a point spacing of 1.98 cm^{-1} over the 5000–4000 cm^{-1} spectral range. In all, 222 spectra were obtained from 111 independent samples collected during 11 separate and unique thinning reactions. All single-beam spectra were subsequently transferred to an Iris Indigo computer (Silicon Graphics, Inc., Mountain View, CA) for spectral processing. Processing of single-beam spectra was accomplished by using software provided by Professor Gary W. Small from the Center for Intelligent Chemical Instrumentation in the Department of Chemistry at Ohio University, Athens, OH. PLS regression and Fourier filtering were performed with the use of the IMSL software package (IMSL Inc., Houston, TX).

RESULTS AND DISCUSSION

Reference Spectrum. The reference spectrum is critical for reproducible results between thinning reactions. In our previous work, the reference spectrum corresponded to a sample taken from the starch slurry immediately before the hydrolysis reaction was initiated.³ More spe-

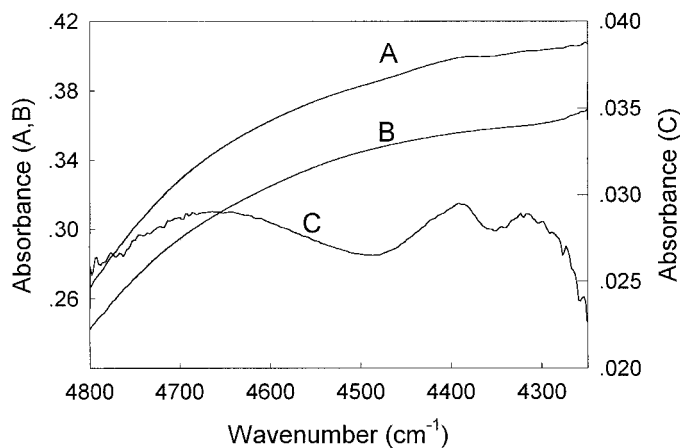


FIG. 1. Absorbance spectra for a sample collected 155 min into the thinning reaction (**A** and **C**). Spectra **A** and **C** are ratioed to the spectrum of sample collected before and after addition of sulfuric acid, respectively. Spectrum **B** corresponds to 0.37 M sulfuric acid ratioed to water.

cifically, this reference sample was collected after the slurry reached the reaction temperature (50–55 °C), but before acid was added to initiate hydrolysis. This reference sample effectively compensates for variations in the amount of soluble carbohydrates in solution prior to the hydrolysis reaction. Soluble carbohydrates result from the dissolution of low-molecular-weight carbohydrates adsorbed onto the suspended starch particles. The amount of soluble carbohydrates varies with each batch of starch feed material.

The reference sample described above is not ideal, because it does not compensate for spectral variations associated with the sulfuric acid, which is necessary to initiate the hydrolysis reaction. Figure 1 shows the effect of sulfuric acid on a typical carbohydrate spectrum. Spectrum **A** corresponds to an absorbance spectrum of a sample collected 155 min after initiating the thinning reaction. This spectrum is produced by using water as the reference solution. Features associated with soluble carbohydrates produced during the thinning reaction are not evident in the resulting ratioed spectrum. Spectrum **C**, on the other hand, is the same sample spectrum, but the reference spectrum corresponds to a solution collected just after initiating the thinning reaction. Specifically, the reference solution used for spectrum **C** is obtained by adding sulfuric acid to the starch slurry, immediately collecting and centrifuging a sample of this acidified slurry, and collecting the NIR single-beam spectrum. A visual comparison of spectra **A** and **C** clearly reveals a dramatic improvement from the use of a better matched reference spectrum. The expected carbohydrate spectral features at 4700, 4400, and 4300 cm^{-1} (2128, 2272, and 2326 nm) cannot be seen in spectrum **A**, but are evident in spectrum **C**. Spectrum **B** shows the absorbance spectrum of a sulfuric acid solution at the same concentration as in the thinning reaction. Water is the reference solution for this spectrum. The similarity between spectra **A** and **B** indicates that the acid is responsible for the broad absorption feature in spectrum **A**. This acid effect is compensated in spectrum **C** by using a reference spectrum collected after acidifying the starch slurry.

The effect of sulfuric acid was examined further by

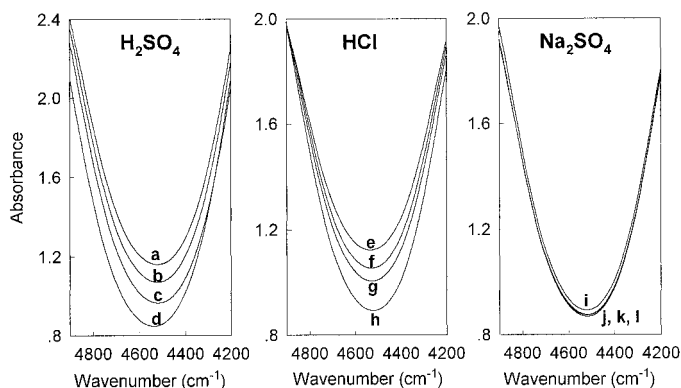


FIG. 2. Absorbance spectra of 0.24 (a), 0.37 (b), and 0.43 (c) M H_2SO_4 ; 0.24 (e), 0.37 (f), and 0.43 (g) M HCl ; and 0.24 (j), 0.37 (k), and 0.43 (l) M Na_2SO_4 . Spectra d, h, and i are absorbance spectra of water.

comparing spectra from different concentrations of sulfuric acid, hydrochloric acid, and sodium sulfate. The main purpose of this examination was to establish whether the absorption features shown in Fig. 1 are caused by sulfate or pH. All the spectra collected are shown in Fig. 2. Each spectrum was ratioed to an air background. No significant difference in absorption is observed for the different concentrations of sodium sulfate. This result clearly indicates that absorption of sulfuric acid in the combination range is not caused by the absorptivity of sulfate. Similar spectral variation is observed, however, for solutions of sulfuric and hydrochloric acid. Absorption of light between the two strong water absorption bands centered at 5200 and 3800 cm^{-1} (1923 and 2631 nm) increases with increasing concentration of each acid. This finding suggests that the effect of pH on the absorptivity of water is involved. As the pH decreases, more protons are present in solution, which alters the extent of hydrogen bonding and affects the water absorption bands. As pH decreases, the water bands are broadened, thereby reducing the optical throughput of the sample between 4800 and 4200 cm^{-1} (2038 and 2380 nm). Consequently, the measured absorbance increases with higher concentrations of sulfuric and hydrochloric acid.

The reference solution used in subsequent experiments corresponds to a sample collected after the starch slurry reached the reaction temperature and immediately following the addition of sulfuric acid to initiate the hydrolysis reaction. Variations in the amount of soluble carbohydrates and sulfuric acid are equally compensated by using this reference solution. A unique reference solution is necessary for each thinning reaction.

PLS Calibration Models. Before PLS regression can be implemented, the entire set of 222 spectra from 111 samples were divided into individual calibration and prediction sets. The calibration set contained 177 spectra and the remaining 45 spectra made up the prediction data set that was used to validate PLS calibration models. Spectra in the prediction set were not included in the calibration set and are selected randomly.

Spectral range and number of factors are critical PLS parameters that must be considered when developing calibration models.^{10,11} The six spectral ranges examined in this study are listed in Table I. These ranges include spe-

TABLE I. PLS calibration results for different spectral ranges using raw absorbance spectra.

Spectral range (cm^{-1})	Number of factors	SEC (mL)	SEP (mL)
4850–4250	7	1.18	1.38
4470–4250	6	1.64	1.42
4850–4350	9	0.97	1.26
4850–4470	13	1.09	1.81
4470–4350	6	1.27	1.56
4350–4250	5	2.57	2.23

cific combinations of the three characteristic absorption bands for carbohydrates (4700 , 4400 , and 4300 cm^{-1}). The widest spectral range tested is $4850\text{--}4250\text{ cm}^{-1}$ ($2062\text{--}2353\text{ nm}$) and incorporates all three carbohydrate bands. Wavenumbers outside this range [$5000\text{--}4850$ and $4250\text{--}4000\text{ cm}^{-1}$ ($2000\text{--}2062$ and $2353\text{--}2500\text{ nm}$) range] are not considered, because no carbohydrate information is present here and strong water absorption at these wavenumbers results in low percent transmission and large spectral noise. The following additional ranges were tested: $4850\text{--}4350$, $4470\text{--}4250$, $4850\text{--}4470$, $4470\text{--}4350$, and $4350\text{--}4250\text{ cm}^{-1}$ ($2062\text{--}2298$, $2237\text{--}2353$, $2062\text{--}2237$, $2237\text{--}2298$, and $2298\text{--}2353\text{ nm}$). The first isolates the 4700 and 4400 cm^{-1} bands and the second isolates the 4400 and 4300 cm^{-1} bands. The last three ranges focus on single bands at 4700 , 4400 , and 4300 cm^{-1} , respectively.

The optimum number of factors can be identified as the number of factors that gives a minimum standard error of prediction (SEP) for a separate set of validation samples not present in the calibration set. SEP is an excellent index to represent the ability of a calibration model to predict analyte concentrations independently. Figure 3 shows standard error of calibration (SEC, open circles) and SEP (filled circles) plotted as functions of the number of PLS factors used for the determination of fluidity within the $4470\text{--}4250\text{ cm}^{-1}$ range. As expected, both the SEC

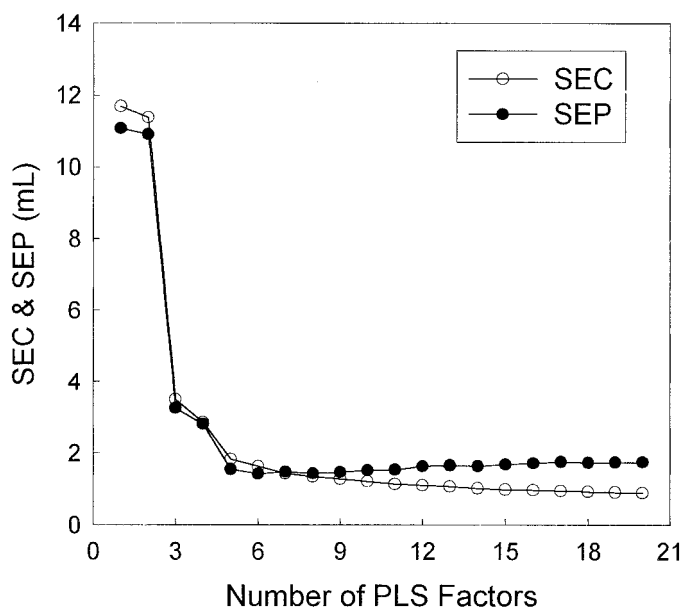


FIG. 3. Effect of PLS factors on SEC and SEP for fluidity measurements over the $4470\text{--}4250\text{ cm}^{-1}$ spectral range.

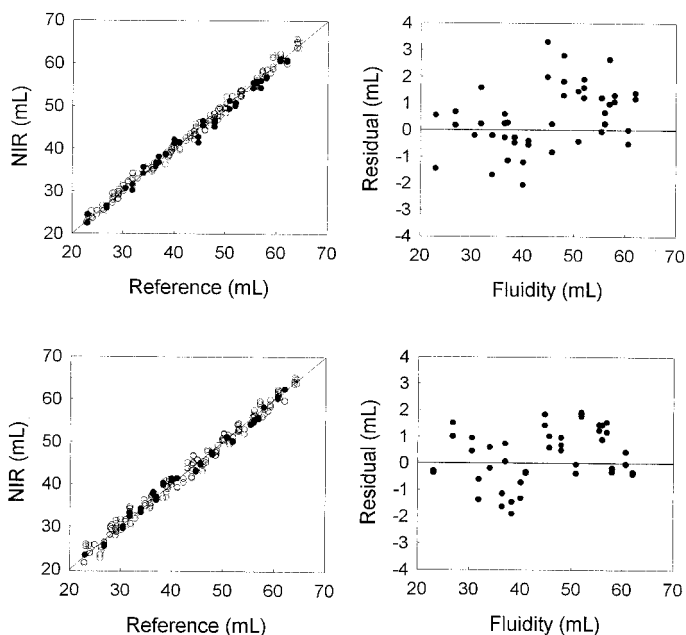


FIG. 4. Fluidity correlation and prediction residual plots using raw (top) and Fourier filtered spectra (bottom) over the 4850–4350 cm^{-1} spectral range. The resulting SEC and SEP are 0.97 mL (R^2 : 0.994) and 1.26 mL (R^2 : 0.958) for raw spectra, and 1.35 mL (R^2 : 0.985) and 1.06 mL (R^2 : 0.972) for Fourier filtered spectra, respectively.

and SEP decrease sharply with the initial factors and gradually decrease as more analyte-dependent spectral variation is incorporated into the calibration model. As the number of factors increases further (i.e., the 7th factor in Fig. 3), the SEC continues to drop slightly while the SEP begins to increase. This type of response is common for factor-based multivariate calibrations. An increase in the SEP indicates that the data are overmodeled by incorporating spectral variation into the calibration model that is not related to fluidity. In this case, the optimum number of factors is six. This same procedure was used to determine the optimum number of factors for each calibration model examined in this work.

Results from PLS calibration models with raw absorbance spectra are summarized in Table I for all spectral ranges. The best calibration model corresponds to the 4850–4350 cm^{-1} range with nine factors. This finding indicated that the 4300 cm^{-1} band adversely affects model performance. Figure 1 shows that the 4300 cm^{-1} band is noisy compared to the other absorption bands; therefore, inclusion of this noisy region, even with the available carbohydrate information, results in worse calibration performance. This finding is consistent with poor SEC and SEP values when the 4300 cm^{-1} band is used alone. No single absorption band outperforms models based on two or three bands. A single carbohydrate band does not provide acceptable calibration results, since each band provides only limited information related to fluidity.

Figure 4 shows the scatter plot showing correlation between reference and NIR fluidity measurements for the nine-factor, 4850–4350 cm^{-1} model (upper left). Open and filled circles represent calibration and prediction data, respectively. The calibration and prediction data correlate well with the conventional reference data, and many points fall on or close to the unity line. A plot of predic-

tion residual vs. reference fluidity is also presented in Fig. 4 (upper right). This plot indicates a slight positive bias in the prediction results. Nevertheless, fluidity values in the prediction data set were predicted with an SEP of 1.26 mL and a mean percent error of 2.28%. This SEP is considerably better than the 1.94 mL obtained with the univariate model.³ Still, a lower SEP is necessary for actual field measurements where a value of 1.0 mL is required. Model performance can be improved by using a digital Fourier filter to reduce spectral noise and baseline variation in the raw absorbance spectra.

PLS Combined with Digital Filtering. Previous work with clinical glucose measurements and NIR spectroscopy demonstrates that digital filtering before PLS regression can significantly improve the prediction accuracy by selectively eliminating spectral noise and baseline variations.^{3,6} The digital filter used in this work is a Fourier filter that selectively passes spectral features according to shape.^{3,6} In the Fourier filtering process, the raw absorbance spectrum is taken as a superposition of sine waves. Noise corresponds to high-frequency sine waves, baseline variations correspond to low-frequency sine waves, and the molecular absorption bands correspond to sine waves with intermediate frequencies. The Fourier transformation process separates this combination of sine waves according to their frequencies (termed digital frequencies). The filtering process involves multiplying the transformed spectrum by a Gaussian-shaped function, thereby weighting the information under the Gaussian. The Gaussian response function is defined by the mean position of the Gaussian curve along the digital frequency axis and the standard deviation of the Gaussian curve, which defines the width of the filter. The mean position must be set properly, so the filter passes absorption features associated with the analyte while discriminating against other spectral features. Width of the Gaussian curve must be set to maximize the analyte-dependent information. If the Gaussian function is too wide, irrelevant information will pass, but if it is too narrow analyte-dependent information will be lost. After the multiplication step, an inverse transform is implemented to return the data to the original domain of an absorbance spectrum.

The key to successful digital filtering is to identify the optimal mean position and standard deviation for the Gaussian filter function. This can be accomplished by constructing and testing PLS models for all combinations of mean position and standard deviation. Spectra are filtered, and the resulting filtered spectra are used to generate a PLS calibration model with a given number of factors and spectral range. An internal validation is required in the filter optimization algorithm. Therefore, 45 out of the original 177 calibration spectra were used as a “monitoring” set to serve as a pseudo-prediction set for filter optimization purposes. Response function for the optimization scheme was computed as the reciprocal of the sum of the mean square calibration error and mean square prediction error ($1/[\text{MSE} + \text{MSPE}]$). MSE was calculated as

$$\text{MSE} = \left[\sum_{i=1}^n (c_i - C_i)^2 \right] / (n - h - l)$$

where n is the number of spectra in the calibration set, h

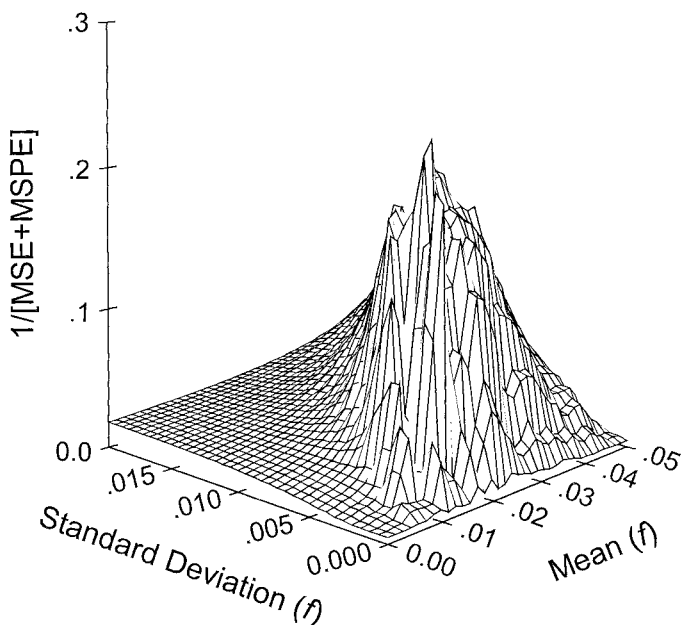


FIG. 5. The response surface map for optimizing the mean and standard deviation for a Fourier filter. Results are presented for a model with four factors over the 4850–4350 cm^{-1} spectral range.

is the number of PLS factors used, c_i is the measured fluidity corresponding to spectrum i , and C_i is the fluidity calculated by the calibration model. MSPE was calculated as

$$\text{MSPE} = \left[\sum_{j=1}^n (m_j - M_j)^2 \right] / n$$

where n is the number of spectra in the monitoring set, m_j is the measured fluidity of spectrum j in the monitoring set, and M_j is the fluidity predicted by the model. A mesh response surface was then generated by plotting response function values vs. the mean positions and standard deviation of the Gaussian filter. The morphology of the surface was examined, and the optimum Gaussian function parameters were identified as the maximum feature on the surface. The highest peak corresponds to the lowest sum of mean square errors of calibration and prediction.

A sample response surface is presented in Fig. 5. This surface is generated by using four factors with the 4850–4350 cm^{-1} spectral range. For this surface plot, response functions are computed for all combinations of means ranging from 0 to 0.05 (0.001 interval) and standard deviations ranging from 0 to 0.02 (0.001 interval), which corresponds to 1000 individual filters. The surface in Fig. 5 shows a maximum at a mean-standard deviation pair of 0.015–0.003 f (digital frequency units). The filter parameters strongly affect calibration performance. Analogous surface plots were generated and examined for the other spectral ranges. In all cases, four-factor models were used to evaluate the surface plots. As discussed elsewhere,^{7,12} too many factors result in broad, ridge-like surface features that make it difficult to identify the ideal filter parameters.

Optimal filter parameters for the different spectral ranges are summarized in Table II. The optimal filter pa-

TABLE II. PLS calibration results for different spectral ranges using Fourier filtering.

Spectral range (cm^{-1})	Mean (f)	Standard deviation (f)	Number of factors	SEC (mL)	SEP (mL)
4850–4250	0.016	0.003	9	1.31	1.10
4470–4250	0.016	0.003	5	1.43	1.25
4850–4350	0.015	0.003	6	1.35	1.06
4850–4470	0.016	0.003	7	1.34	1.15
4470–4350	0.014	0.002	6	1.29	1.26
4350–4250	0.030	0.006	13	1.72	1.51

rameters are similar for the different spectral ranges, which suggests that the spectral features related to fluidity are similar in the digital frequency domain. The results in Table II summarize PLS calibration models over the various spectral ranges with optimized Fourier filters. SEP values are better in all six spectral ranges compared to the analogous PLS models with unfiltered spectra. Models based on Fourier filtered spectra are relatively insensitive to spectral range. Again, the worst results correspond to the 4300 cm^{-1} absorption band. For the most part, lower SEP values are obtained and fewer factors are necessary compared to models from raw spectra.

The best performance was obtained with the 4850–4350 cm^{-1} spectral range, six factors, and a Fourier filter defined by a mean of 0.015 f and a standard deviation of 0.003 f . The corresponding SEP and mean percent error are 1.06 mL and 2.16%, respectively. Figure 4 presents the corresponding scatter and prediction residual plots for this calibration model. The calibration and prediction data fall close to the ideal line with no indication of deviation. In the prediction residual plot, the predicted data are close to the zero residual line with no evidence of a systematic bias. The Fourier filtering step clearly improves model performance and results in SEP values suitable for *on-line* monitoring.

Evaluation of Spectral Acquisition Time on Analytical Performance. Analysis time is critical for a putative *on-line* monitor system. Typically, process control performance is directly influenced by the frequency as well as accuracy of the analytical measurement. In most vibrational spectroscopic methods, analysis time is essentially governed by the time required to collect an individual spectrum. In this study, each single-beam spectrum was collected by coadding 256 interferograms, which took approximately 4 min. The analysis time can be reduced by coadding fewer interferograms. For the evaluation of the relationship between number of coadded interferograms (acquisition time) and resulting SEP, NIR spectra were arbitrarily collected with different number of coadded interferograms (256, 192, 128, and 64). In all, 36 spectra were collected for 18 fluidity values. Fluidity was then predicted from the best calibration model (spectral range: 4850–4350 cm^{-1} , six factors, mean: 0.015 f , standard deviation: 0.003 f) in Table II.

Figure 6 presents 100% lines for water spectra collected with the indicated number of coadded interferograms (top) and the relationship between number of coadded interferograms and measurement SEP and mean percent error (bottom). The 100% lines are offset for clarity. As expected, noise on the 100% lines is lower with more coadded interferograms. Fewer coadded interfero-

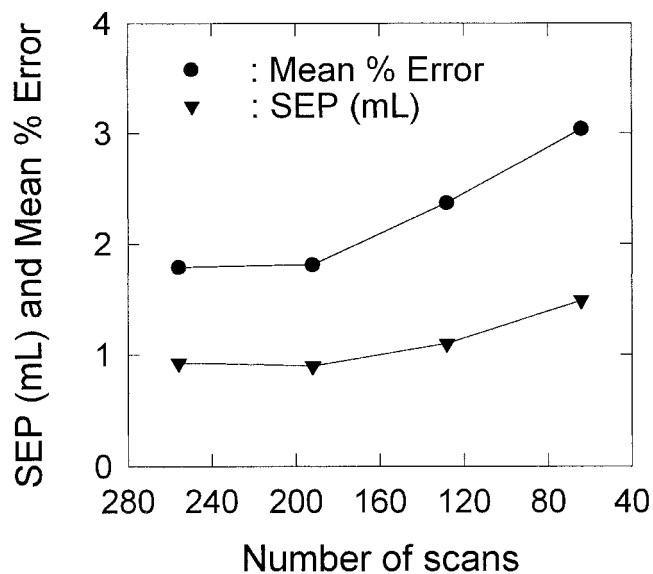
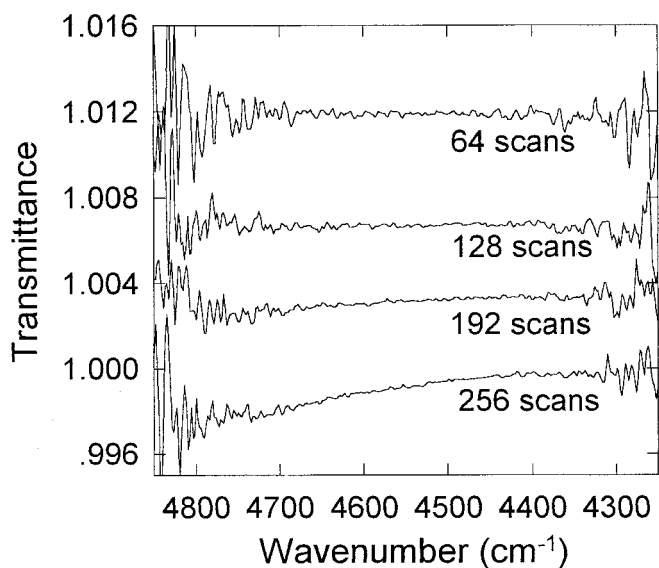


FIG. 6. The 100% lines for water collected with different number of coadded interferograms (top) and effect of coadded interferograms on SEP and mean percent error of the analytical measurement (bottom).

grams (shorter acquisition time) result in greater noise and poorer SEPs and mean percent errors. Although SEPs and mean percent errors are similar for 192 and 256 coadded interferograms, these values increase with 64 and 128 coadded interferograms. A trade-off is necessary between analysis time and prediction accuracy. The data in Fig. 6 show that model performance can be maintained while reducing the acquisition time 4 min (256 coadded scans) to 2 min (196 coadded scans). A further reduction in acquisition time will adversely affect model performance. From an industrial standpoint, a 4 min acquisition interval is sufficient because the thinning of starch is relatively slow kinetically.

Plant Slurry Samples. Up to this point, slurry samples consisted of laboratory preparations. Although these samples simulate plant conditions, it is important to analyze samples collected from the actual plant environment in order to identify unforeseen differences between labora-

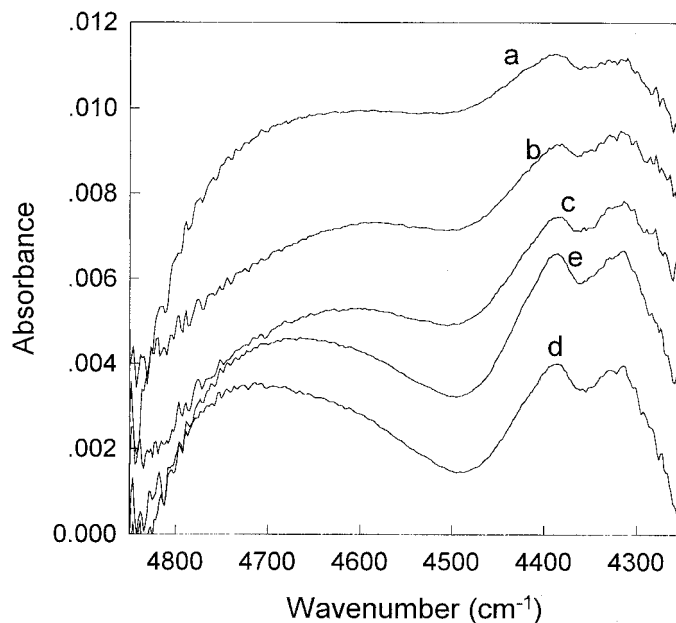


FIG. 7. NIR spectra collected during an actual plant thinning reaction of starch slurry. From a to e, spectra were collected at 125, 150, 200, 250, and 290 min after initiating the thinning reaction, respectively.

tory and plant samples. Plant slurries might contain low concentrations of salts or unidentified substances that significantly alter the NIR spectra. Plant starch slurries were obtained from A. E. Staley Manufacturing Corporation. These samples were collected during two identical, but unique, thinning reactions. Absorbance spectra for one of these reactions are presented in Fig. 7. As before, the reference spectrum corresponds to a single-beam spectrum of the sample collected immediately after adding acid. The characteristic carbohydrate bands at 4700, 4400, and 4300 cm^{-1} are evident, and the absorbance increases as the thinning reaction proceeds. No unusual spectral features or significant spectral differences are evident. Spectral information is essentially identical between laboratory and plant slurry samples. Hence, NIR spectroscopy should be capable of monitoring the hydrolysis of starch for process control.

CONCLUSION

An NIR spectroscopic method has been developed for monitoring starch-thinning reactions. Fluidity was accurately predicted from NIR spectra collected during the starch-thinning reaction. The SEP was 1.06 mL by combining PLS regression with digital Fourier filtering (see Table II). This SEP represents a significant improvement over the univariate model presented before.³ This SEP and the corresponding spectral acquisition time (approximately 4 min) meet the industry standard for an *on-line* monitoring system. No major spectroscopic differences are evident between laboratory and plant slurry samples; therefore, the proposed NIR method appears to be suitable of *on-line* and/or *in-line* analyses for process control of the starch hydrolysis process.

ACKNOWLEDGMENTS

This research was supported by a grant to the University of Iowa from A. E. Staley Manufacturing Corporation. The technical assistance

and insightful comments from Dr. Kenneth Moser are gratefully acknowledged.

-
1. D. A. Burns and E. W. Ciurczak, *Handbook of Near-Infrared Analysis* (Marcel Dekker, New York, 1992).
 2. D. L. Wetzel, *Anal. Chem.* **55**, 1165A (1993).
 3. H. Chung and M. A. Arnold, *Appl. Spectrosc.* **49**, 1097 (1995).
 4. H. Martens and T. M. Næs, *Multivariate Calibration* (John Wiley and Sons, New York, 1989).
 5. K. R. Beebe, R. J. Pell, and M. B. Seasholtz, *Chemometrics: A Practical Guide* (John Wiley and Sons, New York, 1998).

6. M. A. Arnold and G. W. Small, *Anal. Chem.* **62**, 1457 (1990).
7. M. A. Arnold, L. A. Marquardt, and G. W. Small, *Anal. Chem.* **65**, 3279 (1993).
8. G. W. Small, L. A. Marquardt, and M. A. Arnold, *Anal. Chem.* **65**, 3271 (1993).
9. D. Childers and A. Durling, *Digital Filtering and Signal Processing* (West Publishers, St. Paul, Minnesota, 1975).
10. H. Chung, M. A. Arnold, M. Rhiel, and D. W. Murhammer, *Appl. Spectrosc.* **50**, 270 (1996).
11. H. Chung, J. S. Lee, and M. S. Ku, *Appl. Spectrosc.* **52**, 885 (1998).
12. S. Pan, H. Chung, M. A. Arnold, and G. W. Small, *Anal. Chem.* **68**, 1124 (1996).